

NUMERICAL ANALYSIS OF THE ELECTROSPINNING PROCESS FOR FABRICATION OF COMPOSITE FIBERS

by

Adnan AHMED and Lan XU*

National Engineering Laboratory for Modern Silk, College of Textile and Clothing Engineering,
Soochow University, Suzhou, China

Original scientific paper
<https://doi.org/10.2298/TSCI2004377A>

An electrospun composite fiber process is a multi-phase and multi-physics process. It was very difficult to study a charged jet in the electrospinning process for the fabrication of composite fibers by experiments. In this study, the liquid-solid two-phase flow in the electrospinning process for fabrication of composite fibers was researched numerically. The results showed the addition of conductive nanoparticles resulted in the increase of the jet flow velocity, and the decrease of the fiber's diameter. The CFD results corresponded well with the experimental data.

Key words: *electrospinning, composite fibers, numerical simulation*

Introduction

In the electrospinning (ES), an external electric field is applied to overcome the polymer solution surface tension and a charged jet is then ejected from the so-called Taylor cone at the tip of the spinning nozzle [1-10]. The technology has been known as an efficient and simple method for fabricating polymer nanofibers [11, 12]. Composite fibers possess unique surface, bulk and structural properties which make them used widely in various applications, such as filtration, separation, sensor, catalysis, tissue engineering, and drug delivery system [13-15]. Various kinds of composite fiber membranes can also be prepared easily by ES through controlling the spinning parameters, such as additive particles, voltage, flow rate, solvent ratio, solvent evaporation, and humidity [16-21].

The spinning process is a multi-phase and multi-physics process, fig. 1. In this process, the solvent evaporates from the moving jets and a composite fiber membrane is formed on the receptor [22]. Many types of studies, such as experimental research [23-25], theoretical analyses [26-28] and mathematical models [29, 30], have been carried out on the ES nanofiber process. Xu *et al.* [31] modeled ES processes and established a multi-phase model for ES process [32]. Fan *et al.* [33] presented a fluid-mechanic model considering solvent volatilization to research nanopores structure formation in the ES process. Xu [34] established a modified particle suspension model to research the ES process. However, these studies were all about the establishment of mechanic models, which cannot offer in-depth insight into physical understanding of the ES process and also could not numerically simulate the jet flow in the ES process.

* Corresponding author, e-mail: lanxu@suda.edu.cn

In this paper, the liquid-solid two-phase flow in the ES process is researched numerically through using CFD technique to obtain a significant insight of the process, fig. 1. Based on the multi-phase flow model considering solvent volatilization and dispersion of additive particles in our previous work [18-20], the two-phase flow would be simulated by solving numerically the modified Navier-Stokes equations. The CFD simulation results indicated the effects of spinning parameters on the quality of products and they could be applied to gain the optimal spinning parameters for fabrication of electrospun composite fibers.

The 3-D model of the polymer jet in the electrospun composite fiber process

The spinning process was shown in fig. 1. In the experiment, firstly a controlled amount (8 wt.%) of polyvinyl alcohol (PVA) particles were dissolved in the deionized water,

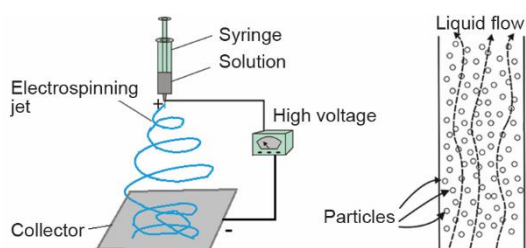


Figure 1. Schematic of the electrospun composite fiber process

then a small amount (0.5 wt.%) of Fe_3O_4 nanoparticles of 20 nm in diameter were dispersed in the already prepared 8 wt.% PVA solution. The density, viscosity and electrical conductivity of the 8 wt.% PVA solutions with and without Fe_3O_4 nanoparticles were shown respectively in tab. 1. The internal diameter of the needle was 0.2 mm. The tip-to-collection distance was 12 cm. The applied voltage was 15 KV. The flow rate was 1.8 mL per hour.

Table 1. Properties characterization of spinning solutions

Spinning solution	Density [kgm^{-3}]	Viscosity [mPas^{-1}]	Electrical conductivity [μscm^{-1}]
Pure PVA solution	1013	317	870
PVA/ Fe_3O_4 solution	1038	476.8	980

Simulation of the polymer jet

The dynamics of the polymer jet in the ES composite fibers process was simulated using CFD. Obviously, dynamical change of the liquid-solid interface in the ES was a crucial phenomenon of the ES process. Therefore, tracking the liquid-solid interface location was very important in numerical simulation. To simulate the mechanism of the jet motion, two different phases including liquid and particles were considered in the simulation. The Lagrangian discrete phase model (DPM), which followed a Euler-Lagrange approach, was adopted in the simulation. In the Euler-Lagrange approach, the liquid was treated mathematically as a continuous phase and the particles were treated as a discrete phase. Therefore, the Navier-Stokes equations were solved for the liquid phase and the motions of particles were followed using Newton's second law.

Equations for the liquid phase

Assuming the jet to be isothermal and ignoring interphase mass transfer, the conservation equations for the q^{th} phase could be written:

– Continuity equation

$$\nabla(\alpha_q \rho_q \mathbf{u}_q) = 0 \quad (1)$$

– Momentum transfer equation

$$\nabla(\alpha_q \rho_q \mathbf{u}_q \mathbf{u}_q - \alpha_q \boldsymbol{\tau}) = -\alpha_q \nabla p + \mathbf{M}_q \quad (2)$$

where α_q is the volume fraction, ρ_q – the density, \mathbf{u}_q – the velocity, $\boldsymbol{\tau}$ – the viscous stress tensor, p – the pressure shared by both fluids, and \mathbf{M}_q – the total interphase force acting on the q^{th} phase.

Equations of motion for particles

A trajectory of a particle by integrating the force balance on the discrete phase, which was written in a Lagrangian reference frame. This force balance, \mathbf{M}_q , equated the particle inertia with the forces acting on the particle and could be written (for the x direction in Cartesian co-ordinates):

$$\frac{du_p}{dt} = F_D(u - u_p) + \frac{g_x(\rho_p - \rho)}{\rho_p} + F_x \quad (3)$$

where $F_D(u - u_p)$ is the drag force per unit particle mass and F_x – an additional acceleration force, which was important in the particle force balance when $\rho > \rho_p$:

$$F_D = \frac{18\mu}{\rho_p d_p^2} \frac{C_D \text{Re}}{24} \quad (4)$$

$$F_x = \frac{1}{2} \frac{\rho}{\rho_p} \frac{d}{dt}(u - u_p) \quad (5)$$

where u is the liquid phase velocity, u_p – the particle velocity, μ – the molecular viscosity of the liquid, ρ – the liquid density, ρ_p – the density of the particle, and d_p – the particle diameter.

Numerical simulation

The variational-based finite element method [35-37] are widely used in numerical methods, however, the present two-phase problem is complex and we have difficulty in establishing a needed variational formulation, so the CFD technique is adopted for this purpose. In the simulation, finite-difference interpolation schemes and the explicit approach were used to solve Navier-Stokes equations. A realizable k - ε model was used to model the turbulent viscosity. In addition, three of CFD sub-models, MHD model, turbulent model and DPM model were applied to simulate the two-phase jet flow numerically.

Computational domain and simulation parameters

The computational domain of the 3-D simulation, as shown in fig. 2, was a circular cylinder with diameter $D = 30$ mm and height $h = 120$ mm. In order to simulate the effect of the addition of Fe_3O_4 nanoparticles on the jet velocity, the following simulation parameters were the PVA solution dynamic viscosity, μ , of 317 mPa·s, the PVA solution electrical conductivity of 870 $\mu\text{s}/\text{cm}$, the PVA solution mass density, ρ , of 1013 kg/m^3 , the Fe_3O_4 particle mass density, ρ_p , of 5180 kg/m^3 , the PVA/ Fe_3O_4 solution dynamic viscosity, μ , of 476.8 mPa·s,

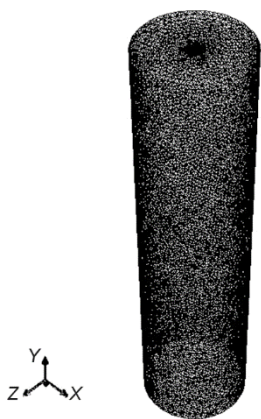


Figure 2. Computational domain and mesh

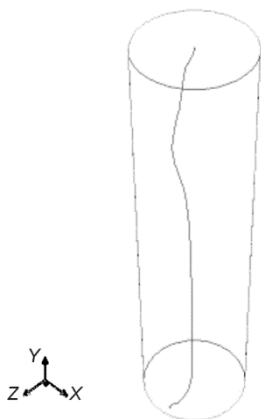


Figure 3. The jet motion in the ES

the PVA/Fe₃O₄ solution electrical conductivity of 980 μs/cm, the PVA/Fe₃O₄ solution mass density, ρ , of 1038 kg/m³, the volume flow rate, Q , of 0.5 mm³/s and the jet unit charge, q , of 300 C/m³.

Boundary conditions

Figure 1 illustrated three boundaries, each boundary condition was set:

- flow inlet: $u_{in} \approx 0.02$ m/s (according to the volume flow rate),
- free surface: zero normal gradients for all variables, $\partial\phi/\partial n = 0$,
- no-slip boundary: zero velocity relative to the wall, $u_{wall} = 0$.

Results and discussion

Figure 3 showed the motion of the jet in the ES, which was traced by a streamline plot. And the effect of the addition of Fe₃O₄ nanoparticles on the jet flow velocity was studied by numerical simulation. The calculated jet flow velocities were indicated in fig. 4. Figure 4(a) illustrated the jet flow velocity of pure PVA solution and fig. 4(b) showed the jet flow velocity of PVA/Fe₃O₄ solution. The results showed the addition of Fe₃O₄ nanoparticles resulted in an increase of the jet flow velocity due to the increase of the electrical conductivity. In addition, in order to obtain more detailed information of PVA/Fe₃O₄ jet flow, the velocities of liquid phase (PVA solution) and solid phase (Fe₃O₄ nanoparticles) were exhibited in fig. 5. It could be seen that the liquid phase and the solid phase had nearly the same velocity due to the uniform distribution of Fe₃O₄ nanoparticles in PVA solution.

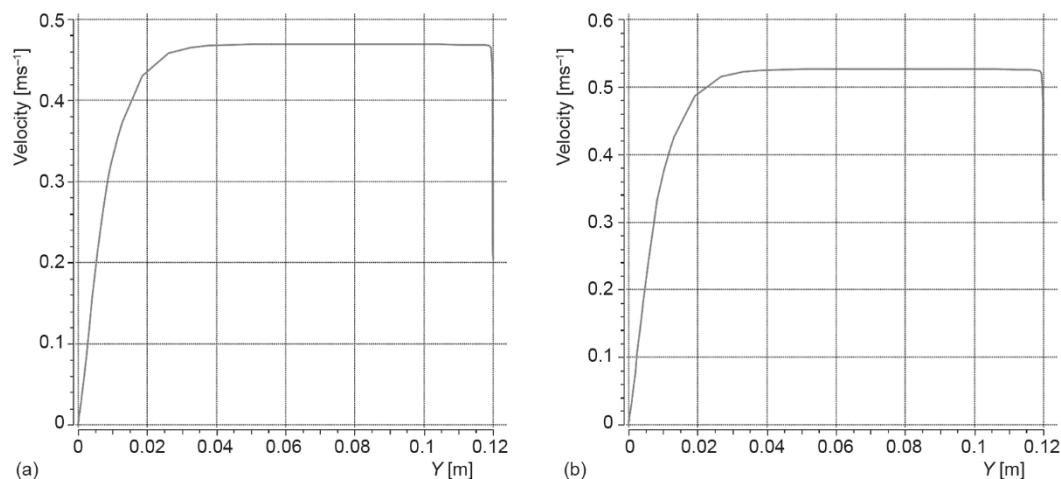


Figure 4. The calculated jet flow velocities of PVA solution (a) and PVA/Fe₃O₄ solution (b)

According to the conservation of mass, $\pi r^2 \rho u = Q$, the diameter of the jet decreased with the increase of the velocity of the charged jet. Therefore, the average diameter of electro-

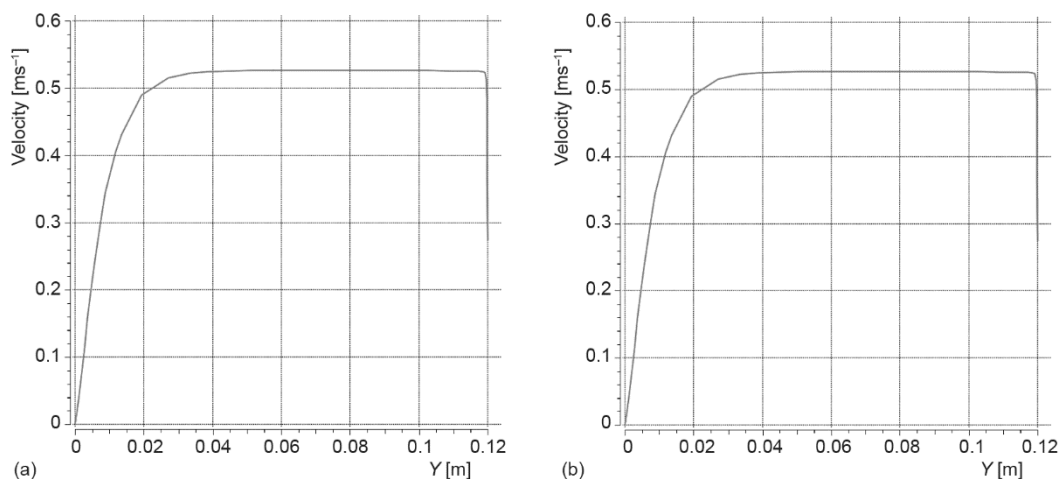


Figure 5. The velocity change vs. spinning distance; (a) liquid phase and (b) solid phase

spun nanofibers would decrease with the increase of the jet velocity, and the average diameter of electrospun PVA/Fe₃O₄ nanofibers was smaller than electrospun PVA nanofibers. The numerical simulation and theoretical analysis results corresponded well to our previous experimental data [10], as shown in tab. 2.

Table 2. The average diameters of electrospun nanofibers [10]

Nanofibers	Average diameter [nm]	Standard deviation [nm ²]	Confidence interval [nm]
PVA	357.5	84.7	±16.6
PVA/Fe ₃ O ₄	320.4	77.3	±15.1

Conclusions

The liquid-solid two-phase flow in the ES composite fibers was researched numerically through using CFD technique to obtain a significant insight of the process. The CFD simulation results indicated the effects of Fe₃O₄ nanoparticles on the quality of product and the addition of Fe₃O₄ nanoparticles resulted in the increase of the jet flow velocity due to the increase of the electrical conductivity. Therefore, the diameter of the jet would decrease as the jet velocity increased according to the conservation of mass, and the average diameter of electrospun PVA/Fe₃O₄ nanofibers was smaller than electrospun PVA nanofibers. The CFD results corresponded well to our experimental data and were reasonable and reliable. In the future, the CFD method will be an effective approach to research ES composite fiber process.

Acknowledgment

The work is supported financially by National Natural Science Foundation of China (Grant No. 11672198), PAPD (A Project Funded by the Priority Academic Program Development of Jiangsu Higher Education Institutions), and Six Talent Peaks Project of Jiangsu Province (Grant No. GDZB-050).

References

- [1] Tian, D., et al., Geometrical Potential and Nanofiber Membrane's Highly Selective Adsorption Property, *Adsorption Science & Technology*, 37 (2019), 5-6, pp. 367-388
- [2] Li, X. X., et al., Nanoscale Adhesion and Attachment Oscillation Under the Geometric Potential, Part 1: The Formation Mechanism of Nanofiber Membrane in the Electrospinning, *Results in Physics*, 12 (2019), Mar., pp. 1405-1410
- [3] He, J. H., et al. Review on Fiber Morphology Obtained by Bubble Electrospinning and Blown Bubble Spinning, *Thermal Science*, 16 (2012), 5, pp. 1263-1279
- [4] Liu, Z., et al., Active Generation of Multiple Jets for Producing Nanofibres with High Quality and High Throughput, *Materials & Design*, 94 (2016), Mar., pp. 496-501
- [5] Liu, Z., et al., Tunable Surface Morphology of Electrospun PMMA Fiber Using Binary Solvent, *Applied Surface Science*, 364 (2016), Feb., pp. 516-521
- [6] Liu, Z., et al., Needle-Disk Electrospinning Inspired by Natural Point Discharge, *Journal of Materials Science*, 52 (2017), 4, pp. 1823-1830
- [7] Li, Y., He, J. H., Fabrication and Characterization of ZrO₂ Nanofibers by Critical Bubble Electrospinning for High-Temperature-Resistant Adsorption and Separation, *Adsorption Science & Technology*, 37 (2019), 5-6, pp. 425-437
- [8] Zhou, C. J., et al., Silkworm-Based Silk Fibers by Electrospinning, *Results in Physics*, 15 (2019), Dec., ID 102646
- [9] Chen, R. X., et al., Numerical Approach to Controlling a Moving Jet's Vibration in an Electrospinning System: An Auxiliary Electrode and Uniform Electric Field, *Journal of Low Frequency Noise, Vibration and Active Control*, 38 (2019), 3-4, pp. 1687-1698
- [10] Zhao, J. H., et al., Needle's Vibration in Needle-Disk Electrospinning Process: Theoretical Model and Experimental Verification, *Journal of Low Frequency Noise, Vibration and Active Control*, 38 (2019), 3-4, pp. 1338-1344
- [11] Bhardwaj, N., et al., Electrospinning: A Fascinating Fiber Fabrication Technique, *Biotechnology Advances*, 28 (2010), 3, pp. 325-347
- [12] He, J. H., et al., Review on Fiber Morphology Obtained by Bubble Electrospinning and Blown Bubble Spinning, *Thermal Science*, 16 (2012), 5, pp. 1263-1279
- [13] Goh, Y. F., et al., Electrospun Fibers for Tissue Engineering, Drug Delivery, and Wound Dressing, *Journal of Materials Science*, 48 (2013), 8, pp. 3027-3054
- [14] Ramakrishna, S. U. B., et al., Nitrogen Doped CNTs Supported Palladium Electrocatalyst for Hydrogen Evolution Reaction in PEM Water Electrolyser, *International Journal of Hydrogen Energy*, 41 (2016), 45, pp. 20447-20454
- [15] Song, Y. H., Xu, L., Permeability, Thermal and Wetting Properties of Aligned Composite Nanofiber Membranes Containing Carbon Nanotubes, *International Journal of Hydrogen Energy*, 42 (2017), 31, pp. 19961-19966
- [16] Sun, Z. Y., et al., Characterization and Antibacterial Properties of Porous Fibers Containing Silver ions, *Applied Surface Science*, 387 (2016), Nov., pp. 828-838
- [17] Song, Y. H., et al., Preparation and Characterization of Highly Aligned Carbon Nanotubes/Polyacrylonitrile Composite Nanofibers, *Polymers*, 9 (2017), 1, ID 1
- [18] Wang, Y. R., Xu, L., Preparation and Characterization of Porous Core-Shell Fibers for Slow Release of Tea Polyphenols, *Polymers*, 10 (2018), 2, ID 144
- [19] Peng, N. B., et al., A Rachford-Rice Like Equation for Solvent Evaporation in the Bubble Electrospinning, *Thermal Science*, 22 (2018), 4, pp. 1679-1683
- [20] Liu, L. G., et al., Solvent Evaporation in a Binary Solvent System for Controllable Fabrication of Porous Fibers by Electrospinning, *Thermal Science*, 21 (2017), 4, pp. 1821-1825
- [21] Zhao, L., et al., Sudden Solvent Evaporation in Bubble Electrospinning for Fabrication of Unsmooth Nanofibers, *Thermal Science*, 21 (2017), 4, pp. 1827-1832
- [22] Xu, L., et al., Effect of Humidity on the Surface Morphology of a Charged Jet, *Heat Transfer Research*, 44 (2013), 5, pp. 441-445
- [23] Zhao, J. H., et al., Experimental and Theoretical Study on the Electrospinning Nanoporous Fibers Process, *Materials Chemistry and Physics*, 170 (2016), 6, pp. 294-302
- [24] Liu, H. Y., et al., Effect of Fe₃O₄ Nanoparticles on Magnetic Electrospun Nanofibers, *The Journal of The Textile Institute*, 106 (2015), 5, pp. 503-509

- [25] Zhao, J. H., et al., Effect of Surface-Active Agent on Morphology and Properties of Electrospun PVA Nanofibres, *Fibers and Polymers*, 17 (2016), 6, pp. 896-901
- [26] Tang, X. P., et al., Effect of Flow Rate on Diameter of Electrospun Nanoporous Fibers, *Thermal Science*, 18 (2014), 5, pp. 1439-1441
- [27] Shao, Z. B., et al., Formation Mechanism of Highly Aligned Nanofibers by a Modified Bubble-Electrospinning, *Thermal Science*, 22 (2018), 1A, pp. 5-10
- [28] Zhao, J. H., et al., Preparation and Formation Mechanism of Highly Aligned Electrospun Nanofibers Using a Modified Parallel Electrode Method, *Materials & Design*, 90 (2016), Jan., pp. 1-6
- [29] Xu, L., et al., Theoretical Model for the Electrospinning Nanoporous Materials Process, *Computers and Mathematics with Applications*, 64 (2012), 5, pp. 1017-1021
- [30] Xu, L., et al., A Thermo-Electro-Hydrodynamic Model for Vibration-Electrospinning Process, *Thermal Science*, 15 (2011), Suppl. 1, pp. S131-S135
- [31] Xu, L., et al., A Mathematical Model for Electrospinning Process Under Coupled Field Forces, *Chaos Solitons Fractals*, 42 (2009), 3, pp. 1463-1465
- [32] Xu, L., et al., A Multi-Phase Flow Model for Electrospinning Process, *Thermal Science*, 17 (2013), 5, pp. 1299-1304
- [33] Fan, C., et al., Fluid-Mechanic Model for Fabrication of Nanoporous Fibers by Electrospinning, *Thermal Science*, 21 (2017), 4, pp. 1621-1625
- [34] Xu, L., A Particle Suspension Model for Nanosuspensions Electrospinning, *Thermal Science*, 22 (2018), 4, pp. 1707-1714
- [35] He, J. H., A Modified Li-He's Variational Principle for Plasma, *International Journal of Numerical Methods for Heat and Fluid Flow*, On-line first, <https://doi.org/10.1108/HFF-06-2019-0523>, 2019
- [36] He, J.H. Lagrange Crisis and Generalized Variational Principle for 3-D Unsteady Flow, *International Journal of Numerical Methods for Heat and Fluid Flow*, On-line first, <https://doi.org/10.1108/HFF-07-2019-0577>, 2019
- [37] He, J. H., Sun, C., A Variational Principle for a Thin Film Equation, *Journal of Mathematical Chemistry*, 57 (2019), 9, pp. 2075-2081